Metasurface-Assisted Passive Wireless Communication with Commodity Wi-Fi Signals

Hanting Zhao[1+], Ya Shuang[1+], Menglin Wei[1], Tie Jun Cui[2], Philipp del Hougne[3], and Lianlin Li[1]

[1] State Key Laboratory of Advanced Optical Communication Systems and Networks, Department of Electronics, Peking University, Beijing 100871, China

[2] State Key Laboratory of Millimeter Waves, Southeast University, Nanjing 210096, China

[3] Institut de Physique de Nice, CNRS UMR 7010, Université Côte d'Azur, Nice 06108, France

[+] These authors contributed equally to this work.

Abstract

Wireless communication has become a standard solution to address ever-increasing demands for information transfer in our modern society. Conventional systems work in an ***active*** way in the sense that an active carrier signal is mandatorily required to transfer information from Alice to Bob. Especially in the era of 5G/6G and with the advent of the Internet of Things (IoT), an exponential growth of users and connectivity confronts conventional systems with important challenges including limited spectrum resources, information security, energy consumption and cost efficiency. Here, we introduce the fundamentally different concept of ***passive*** wireless communication (PWC) which has the potential to resolve the above-mentioned issues. PWC transfers digital information by modulating/demodulating already existing omnipresent ambient stray electromagnetic waves using a programmable metasurface. We provide a theoretical framework for encoding/decoding and modulating/demodulating in PWC and build a proof-of-principle prototype system leveraging existing commodity 2.4GHz Wi-Fi signals. We demonstrate information transfer from Alice to Bob with data rates on the order of hundreds of Kbps using distinguishable information-carrying control coding patterns of the metasurface, neither necessitating an active carrier signal and its associated radio-frequency chain nor affecting the background active wireless communication. The presented strategy is particularly appealing for “green” IoT connectivity. At the same time, the concept is applicable to all types of wave phenomena and provides a fundamentally new perspective on the design of future wireless communication architectures.

Introduction

Pioneered by Guglielmo Marconi's discovery of wireless telegraphy in 1897,[1] wireless communication with electromagnetic signals has become a standard approach to transfer information. Typically, a wireless communication system requires the active generation of a high-frequency carrier signal to deliver the information to be conveyed from Alice to Bob[2,3]. For this reason, we would like to refer to such schemes as *active wireless communication* (AWC). The capacity to transfer information with AWC is ultimately bounded by the number of available channels, for instance, how many independent spectral and spatial degrees of freedom there are available[4,5]. To meet the ever-expanding demand for more information transfer, notably given the advent of the Internet of Things (IoT), a wide range of solutions have been proposed, including elaborate coding schemes (e.g. OFDM[6]), elaborate antenna designs (e.g. massive MIMO[7]) and even the engineering of the propagation medium's disorder[8]. Nonetheless, fundamental challenges related to the need for an active carrier signal generation remain: costly and heavy hardware (oscillators, nonlinear mixers, wideband power amplifiers, …), power consumption, spectrum allotment issues and information security. These issues are particularly pressing for IoT connectivity since IoT devices should be lightweight, cheap and "green".

To fundamentally address these challenges, here we propose *passive wireless communication* (PWC). Rather than launching an active carrier signal, the proposed PWC scheme relies on manipulating already existing electromagnetic waves: digital information is encoded into omnipresent stray ambient waves on the physical level using a home-made programmable metasurface[9,10] in an inexpensive and dynamic manner. PWC recycles already existing waves, thereby removing the need for energy, spectral resources and expensive and cumbersome hardware needed to generate carrier signals. Therefore, PWC opens up a promising route toward green IoT connectivity and beyond.

In this article, we introduce a theoretical framework for encoding/decoding and

modulation/demodulation in the proposed PWC paradigm, we design an inexpensive programmable metasurface operating at 2.4GHz, and we build a proof-of-principle PWC prototype system leveraging existing commodity 2.4GHz Wi-Fi signals. Our experiments demonstrate wireless communication without any active radio components at data rates on the order of hundreds of Kbps. The presented PWC strategy provides a fundamentally new perspective on wireless communication and can be transposed to other frequencies[11–13] and other types of wave phenomena.

Results

The proposed PWC is conceptually inspired by passive imaging schemes which are widely utilized in the areas of radar and seismic exploration[14–18]. Passive imaging seeks to locate or detect an object of interest based on clutter signals or background noise and requires a directional reference antenna for calibrating the non-cooperative illumination signal, or an antenna array for retrieving a so-called response matrix. In contrast, the proposed PWC relies on the reallocation of ambient stray electromagnetic waves through an inexpensive programmable metasurface. The programmable metasurface consists of a two-dimensional (2D) array of electronically-controllable digital meta-atoms[9]. For example, a 1-bit meta-atom has two digitalized states, i.e., “0” and “1”, corresponding to two opposite electromagnetic responses. Hence, digital information can be assigned to the meta-atom such that it is directly encoded into the metasurface on the physical level. By now, programmable metasurfaces have found various valuable applications, for instance in programmable electromagnetic imaging and sensing[19–25], wireless communication[8,26–31], dynamic holograms[32], wireless energy deposition[33,34] and analog computation with indoor Wi-Fi infrastructure[35]. The proposed PWC paradigm utilizes the programmable metasurface for three major purposes: (i) encoding the digital information to be conveyed on the physical level; (ii) directly modulating the ambient stray electromagnetic waves with high

signal-to-noise ratio (SNR); and (iii) facilitating the retrieval of digital information encoded into the metasurface with a matching classifier or decoder.

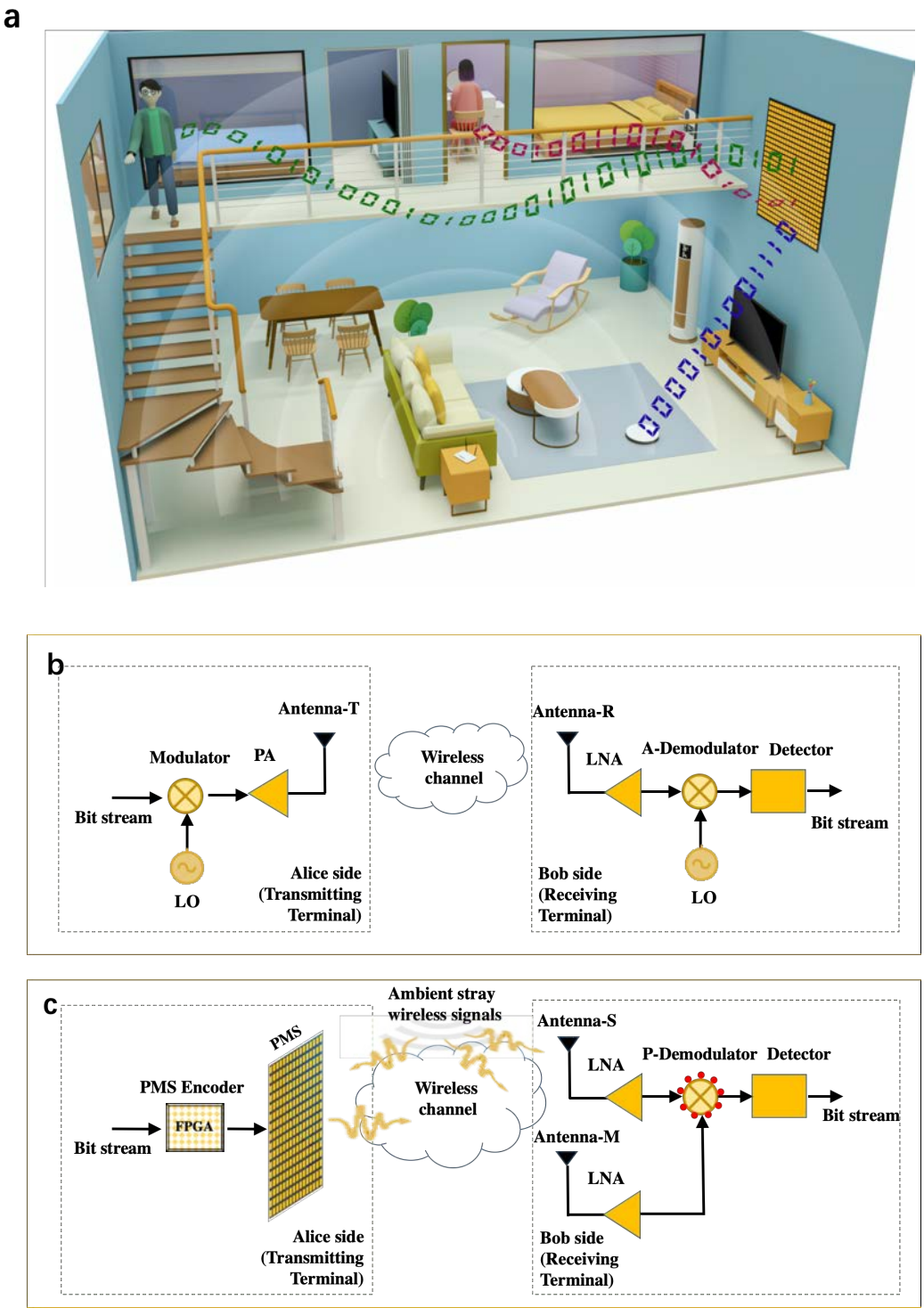

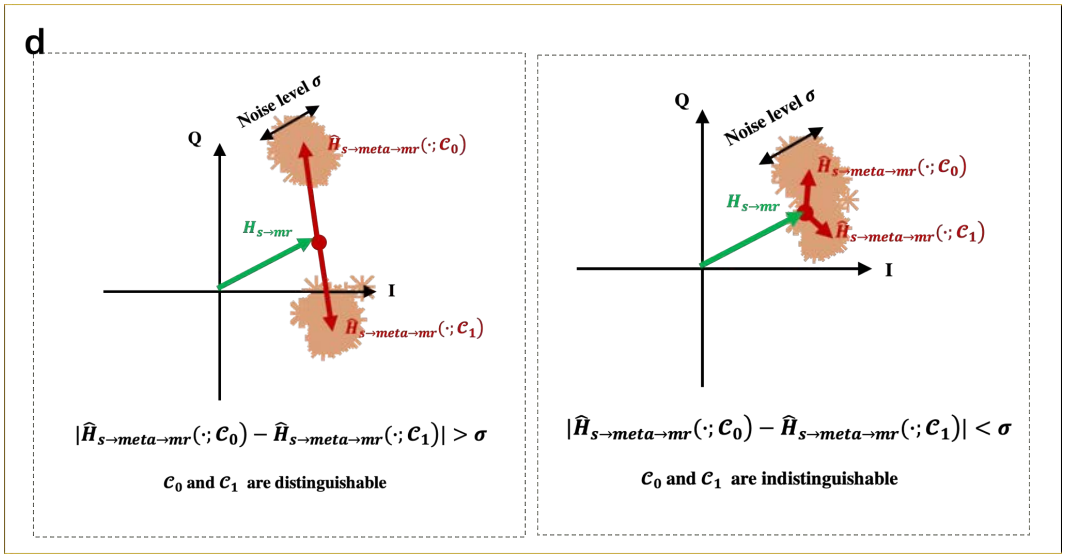

Figure 1. Principle of the proposed PWC. a, An illustrative scenario for the proposed PWC in a typical indoor environment. Here, a programmable metasurface partially decorating the wall transmits simultaneously three direction-dependent streams of digital information to three users (two people upstairs and a robot in the living room) by modulating the ambient stray electromagnetic waves. **b,** Block diagram for AWC. **c**, Block diagram for the proposed PWC. The Programmable MetaSurface (PMS) based encoder maps the digital bit "0" ("1") to the metasurface configuration $\mathcal{C}_0$ ($\mathcal{C}_1$). LO: local oscillator generating the active carrier signal; PA: wideband power amplifier; Antenna-T: transmitting antenna; Antenna-R: receiving antenna; LNA: low-noise amplifier; A-demodulator: AWC demodulator; Antenna-S: slave antenna; Antenna-M: master antenna; P-demodulator: PWC demodulator. **d**, Constellation of the demodulated signals when the programmable metasurface is controlled by the distinguishable (left) and indistinguishable (right) coding patterns. This illustration considers binary phase shift keying modulation; other cases can be found in **Supplementary Note 2**.

PWC system configuration. For simplicity, we consider PWC with binary information quantization as an illustrative example; however, the reported methods and results can be readily extended to multi-level cases. Furthermore, we assume that the information to be conveyed has been processed using standard source coding and channel coding techniques. As shown in **Figure 1c**, the proposed PWC system is composed of four major building blocks: programmable-metasurface-encoder, modulator, demodulator and detector. Modulation/demodulation in PWC is made with respect to an *unknown stray* wireless signal, as opposed to the use of *prior-known local* active carrier in AWC. To address this

difficulty, we explore the unique capability of the programmable metasurface to 'reallocate' the energy of stray wireless waves dynamically and arbitrarily towards desired spots. Using a programmable metasurface, the wireless deposition of energy at desired locations can be enhanced significantly without extra energy consumption[33]. By modulating the stray wireless signal on Alice's side, energy can be 'reallocated' on Bob's side for demodulation provided Bob sits within the corresponding focal spot. Thereby, information can be "sneakily" transferred from Alice to Bob with very high signal-to-noise ratio (SNR), and this PWC has nearly no effect on the background AWC.

On Alice's side, information encoding and signal modulation are realized by the metasurface. To that end, two "distinguishable" digital metasurface coding patterns $\mathcal{C}_0$ and $\mathcal{C}_1$ are designed offline by solving a constrained optimization problem (see **Supplementary Notes 3-4**). For m-level information quantization and k independent channels (or k single-channel users), at least 2^{mk} control coding patterns are needed. "Distinguishable" here refers to the ability to distinguish the two coding patterns based on the stray wireless signals acquired and decoded or classified on Bob's side. For instance, the two control coding patterns $\mathcal{C}_0$ and $\mathcal{C}_1$ can be optimized such that the corresponding acquired wireless signals on Bob's side, after background removal or median filtering, have a phase difference of 180°. During operation, the sequence of digital information to be conveyed is sequentially mapped to that of the "distinguishable" coding patterns. For instance, the digital information "0" ("1") is mapped to $\mathcal{C}_0$ ($\mathcal{C}_1$), and thereby *directly* encoded into the programmable metasurface's physical layer in a time-sequential manner using a field programmable gate array (FPGA). Alice's bit stream can be retrieved by analyzing the sequence of the coherence coefficients on Bob's side, in the above-mentioned example with a standard binary phase shift keying (BPSK) decoder – see details in **Supplementary Note 1**.

Retrieving the digital information from the acquired seemingly random wireless signals on Bob's side is nontrivial, since the carrier signal, i.e., the ambient stray wireless

signal, is typically unknown to Alice and Bob. To address this difficulty, we deploy (at least) two coherent receivers on Bob's side to acquire the ambient stray wireless signals. The stray ambient wireless signals are only focused on one "master" receiver which is hence "visible" to the metasurface; in contrast, a second "slave" receiver is "invisible" to the metasurface and does not capture Alice's information. The unknown modulation signal can automatically be calibrated out using multiple coherent receivers, as detailed in the next section. The focusing of the stray wireless signal on the master receiver is modulated to transfer Alice's information, yielding a high SNR demodulated signal thanks to the strong focusing ability. At the same time, the proposed PWC scheme is expected to virtually not affect the background AWC.

PWC operational principle. For simplicity, let us assume that an unknown wireless source emits a seemingly random signal $s(t)$, and the sequence of binary digital information to be transferred from Alice to Bob is denoted by $g(\tau)$. Since the time-dependent changes in $g(\tau)$ are remarkably slower than those in $s(t)$, we refer to the time τ in $g(\tau)$ as the slow time; and the time t in $s(t)$ as the fast time. In analogy with AWC, $s(t)$ and $g(\tau)$ can be correspondingly regarded as the passive carrier and the modulation signal for PWC, respectively. We need to convert the sequence of binary information $g(\tau)$ into that of the distinguishable information-carrying control coding patterns of the programmable metasurface $\mathcal{C}(\tau)$. At any given slow time τ_0, $\mathcal{C}(\tau_0) = \mathcal{C}_0$ if $g(\tau_0) = 0$ and $\mathcal{C}(\tau_0) = \mathcal{C}_1$ if $g(\tau_0) = 1$. The stray wireless signal y_m acquired by the master receiver at $\boldsymbol{r}_m$ is the superposition of the direct arrival of the stray wireless signal and its reflection off the information-carrying metasurface, namely,

$$y_m(\tau, \boldsymbol{r}_m, \omega) = \tilde{s}(\omega) H_{s\to mr}(\boldsymbol{r}_m, \omega) + \tilde{s}(\omega) H_{s\to meta\to mr}(\boldsymbol{r}_m, \omega; \mathcal{C}(\tau)). \quad (1)$$

Here, $H_{s\to meta\to mr}(\boldsymbol{r}_m, \omega; \mathcal{C}(\tau))$ represent the response of the channel from the unknown wireless source to the master receiver via the $\mathcal{C}(\tau)$-controlled programmable metasurface, and $\tilde{s}(\omega)$ is the frequency-domain representation of $s(t)$. In contrast, the slave receiver at $\boldsymbol{r}_s$ only acquires the direct arrival of stray wireless signal since it is "invisible" to the

metasurface, i.e.,

$$y_s(\tau, \boldsymbol{r}_s, \omega) = \tilde{s}(\omega) H_{s\to sr}(\boldsymbol{r}_s, \omega), \tag{2}$$

where $H_{s\to mr}$ (resp. $H_{s\to sr}$) characterizes the response of the wireless channel from the unknown source to the master (resp. slave) receiver. Then, the normalized coherence coefficient of the two acquired wireless signals reads (see **Supplementary Note 1**):

$$\frac{\langle y_m y_s^* \rangle}{\langle |y_s^*|^2 \rangle} = \widehat{H}_{s\to mr} + \widehat{H}_{s\to meta\to mr}\big(\boldsymbol{r}_m, \omega; \mathcal{C}(\tau)\big), \tag{3}$$

where $\widehat{H}_{s\to mr} = \frac{H_{s\to mr}}{H_{s\to sr}}$ and $\widehat{H}_{s\to meta\to mr} = \frac{H_{s\to meta\to mr}}{H_{s\to sr}}$. At this stage, three conclusions can be drawn from equation (3). First, $H_{s\to meta\to mr}$ as a function of $\mathcal{C}(\tau)$ carries the digital information to be conveyed by Alice, and meanwhile it is almost independent of the unknown wireless signal. Thus, we can interpret $H_{s\to meta\to mr}$ as the demodulated PWC signal. Hence, equation (3) describes the PWC demodulation and equation (1) the PWC modulation procedure. Second, the terms $\widehat{H}_{s\to mr}$ and $\frac{1}{H_{s\to sr}}$ are essentially independent of the slow time τ, thus $H_{s\to meta\to mr}$ can be easily retrieved by using background removal, bandpass pass filtering, or other simple signal processing operations. Third, the binary digital information expressed through the classes of $\mathcal{C}_i (i = 0\ or\ 1)$ can be retrieved by distinguishing $H_{s\to meta\to mr}(\cdot; \mathcal{C}_0)$ from $H_{s\to meta\to mr}(\cdot; \mathcal{C}_1)$. As discussed in **Methods** and **Supplementary Note 1**, the demodulated signal $H_{s\to meta\to mr}$ reflects approximately the wavefield component radiated from the metasurface. In order to make $H_{s\to meta\to mr}(\cdot; \mathcal{C}_0)$ and $H_{s\to meta\to mr}(\cdot; \mathcal{C}_1)$ distinguishable in a robust way, the intensity of the signal component reflected from the metasurface needs to be comparable to that of the direct arrival from the unknown wireless source. This physical constraint can be readily realized by controlling the coding pattern of the programmable metasurface such that the energy of the stray wireless signal carrying the Alice's information is well focused and enhanced around the master receiver. In this way, $|\widehat{H}_{s\to meta\to mr}|$ can be sufficiently bigger than a decision threshold, as shown in **Figure 2d**, which enables robust information retrieval. More details, for instance, for the case of distributed non-cooperative wireless

sources, can be found in **Supplementary Notes 1-3**.

Before closing this section, we briefly comment on the privacy of the presented PWC scheme. Since Alice's information is encoded in the modulation of the focusing on the master receiver, the information cannot be retrieved at remote locations outside the focal spot (see also **Methods**). Moreover, an eavesdropper at a remote location may be deliberately deceived by Alice since the metasurface is capable of generating a number of controllable radiation beams each carrying independent streams of information. For instance, Alice can send deceitful information to an eavesdropper in an undesirable direction which may sharply differ from the information received by Bob. PWC will thus enable novel routes to very-high-privacy wireless communication.

Design of the programmable metasurface and information-carrying control coding patterns. The crucial component of PWC is the programmable metasurface controlled with the distinguishable information-carrying coding patterns. We design an electronically-controllable programmable metasurface, and develop an efficient optimization algorithm for finding the associated control coding patterns. For our proof-of-concept experiments, the metasurface is designed for operation around 2.4GHz which corresponds to the frequency range of commodity Wi-Fi signals. The designed metasurface is composed of 24×32 phase-binary reflection-type meta-atoms. Each meta-atom ($54\text{mm} \times 54\text{mm}$) has two binary states, "0" and "1", corresponding to two opposite reflection phases, i.e., 0 and π, respectively, upon plane wave illumination. Switching between these two states is easily realized by changing the external DC voltage applied to the PIN diode between 3.3V and 0V. In our design, due to fabrication constraints, the entire programmable metasurface is composed of 3×4 metasurface panels, each panel containing 8×8 meta-atoms. Each metasurface panel is equipped with eight identical 8-bit shift registers (SN74LV595APW), and the eight PIN diodes are controlled sequentially. In our design, the adopted clock (CLK) rate is 50MHz, and the switching time of the control coding patterns of the metasurface is about 20μs. More details on the metasurface design

can be found in **Methods** and **Supplementary Note 3**.

As noted above, the coding patterns are optimized to have two important properties: distinguishability and "(in)visibility". For PWC with binary information quantization, identifying the control coding patterns can be formulated as a constrained optimization problem:

$$min_{\mathcal{C}_0,\mathcal{C}_1}\left\{\left\||H^{cal}_{s\to meta\to mr}(.;\mathcal{C}_0)|-|H^{des}|\right\|_2^2+\left\||H^{cal}_{s\to meta\to mr}(.;\mathcal{C}_1)|-|H^{des}|\right\|_2^2\right\} \quad (4)$$

$$\text{s.t.,}\ \frac{f\left(H^{cal}_{s\to meta\to mr}(.;\mathcal{C}_0)\right)}{f\left(H^{cal}_{s\to meta\to mr}(.;\mathcal{C}_1)\right)}\geq\eta.$$

As detailed in **Supplementary Note 1** and **Methods**, the demodulated signal $H_{s\to meta\to mr}$ approximately corresponds to the signal radiated from the programmable metasurface, such that $H^{cal}_{s\to meta\to mr}$ can be treated as the radiation beam from the metasurface. The objective function is minimized such that the information-carrying beam $|H^{cal}_{s\to meta\to mr}(\mathcal{C}_i)|$ (i=0 or 1) is consistent with the desired radiation beam $|H^{des}|$, when the metasurface is controlled by the pattern $\mathcal{C}_i$. The desired beam $|H^{des}|$ is "visible" to (focused on) the master receiver, while being "invisible" to (not focused on) the slave receiver. In addition, the inequality constraint in equation (4) explicitly imposes the property that the adopted information-carrying coding patterns of $\mathcal{C}_0$ and $\mathcal{C}_1$ are distinguishable. This constraint comes from the famous Neyman-Pearson decision rule,[36,37] where η denotes a decision threshold, and a nonlinear function f is introduced to extract the features of the input argument. More details about equation (4) for specific modulation schemes are provided in **Supplementary Note 4**.

Experimental validation of ASK in PWC. For a first proof-of-concept experiment in our indoor laboratory environment, we consider PWC with binary amplitude-shift keying (BASK) (de)modulation by leveraging stray Wi-Fi signals. Unlike AWC-BASK, PWC-BASK means that the demodulated signal's amplitude, i.e., $|\widehat{H}_{s\to meta\to mr}|$, has two digital states, "0" and "1", corresponding to the relatively high (i.e., $\left|\widehat{H}_{s\to meta\to mr}\right|>\eta$) and low

energy levels ($\left|\widehat{H}_{s\to meta\to mr}\right| \leq \eta$), respectively, where η denotes a decision threshold. To demonstrate the capability of the proposed PWC scheme to transfer direction-dependent digital information, we consider a three-channel PWC with 3 access users (Bob-R, Bob-G, Bob-B), as shown in **Figure 2a**.

In an offline calibration step, we identify 2^3 coding patterns of the programmable metasurface by solving the optimization problem in equation (4). As detailed in **Supplementary Note 3**, we approximate the propagation medium as free space. Given the line-of-sight between metasurface and master receivers, this approximation yields good results, as evidenced by the field scans presented in **Supplementary Note 3** which are in good agreement with the simulated spatial distributions of $|\widehat{H}_{s\to meta\to mr}|$ at a distance of z=3m away from the metasurface (shown in F**igure 2c**). In future work, refining the propagation model, e.g. with a learned forward model[25], may further improve the performance of PWC. During operation, we establish the programmable-metasurface-encoding scheme by mapping the three-channel binary information stream to control coding patterns of the metasurface, as reported in **Figure 2b**.

Based on this PWC information encoding scheme, we transmit a full-color image to Bob by simultaneously sending three monochrome images to Bob-R, Bob-G and Bob-B. In our experiments, we connect four commercial electrically-small antennas (one slave antenna and three master antennas) to the input ports of an oscilloscope (Agilent MSO9404A) to acquire the stray Wi-Fi signals modulated by the digital information encoded into the metasurface. The obtained results are reported in **Figure 2d**.

We also investigate the effect of the Wi-Fi router's distance from the metasurface on PWC. Experimental results for three additional distances (1.2m, 4m, and 5m) are reported in **Supplementary Note 6**. The PWC quality decreases as the router's distance increases, since the intensity of the Wi-Fi signals modulated by the metasurface, i.e., $|\widehat{H}_{s\to meta\to mr}|$, decreases correspondingly. Specifically, upon increasing the distance from 1.2m to 5m in our experiment results in an increase of the bit error rate (BER) by 7% on average, as

detailed in **Supplementary Note 6**. Of course, a more specialized en(de)coder can be expected to improve the communication quality. To summarize, the above-reported results evidence the ease of implementing PWC-BASK by manipulating ambient commodity Wi-Fi signals with a carefully configured programmable metasurface.

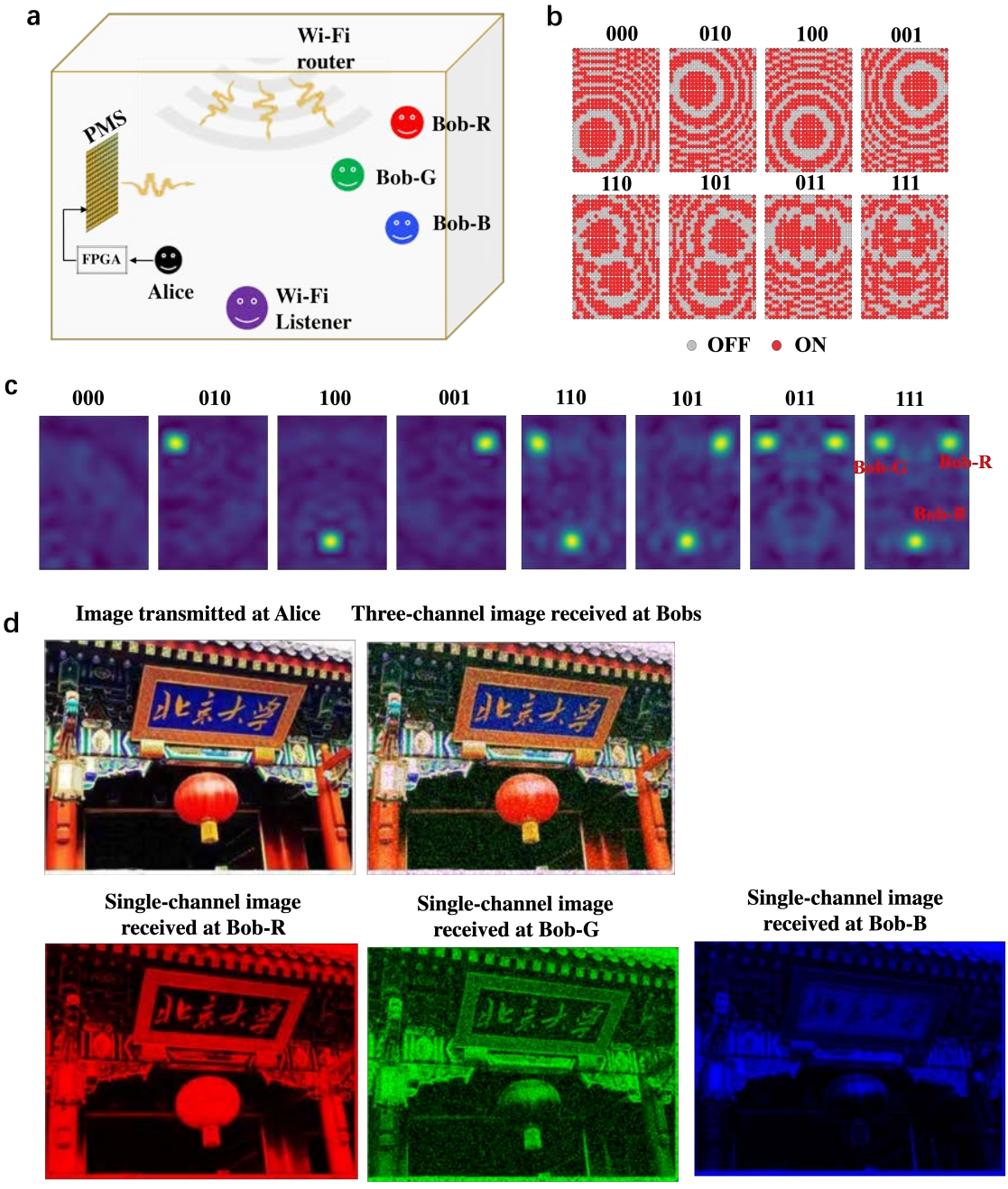

Figure 2. Results of the three-channel BASK PWC. a, Schematic of the experimental setup considering a scenario with commodity Wi-Fi signals in an indoor environment. A 2.412GHz Wi-Fi

router located at an arbitrary location emits radio waves which are captured by a standard AWC Wi-Fi user ("listener"). Alice transmits her three direction-dependent streams of information to three independent users, i.e., Bob-R (-0.86m, 0m, 3m), Bob-G (0.81m, 0.648m, 3m), and Bob-B (0.81m, -0.648m and 3m), by encoding the information into the programmable metasurface, and using it to modulate the stray Wi-Fi waves. The three independent users are located at a distance z=3m away from the metasurface. **b,** Optimized control coding patterns for the three-channel PWC-BASK. **c,** Simulated distributions of $|H_{s\to meta\to mr}|$, corresponding to the eight coding patterns plotted in **b**, for 2.424 GHz at the distance of z=3m from the metasurace. The intensity of stray Wi-Fi signals is well-controlled for the purpose of passive amplitude modulation. **d,** Individual images retrieved by Bob-R, Bob-G, and Bob-B. In addition, the full-color image transmitted by Alice, and the one synthetized using Bob's results are shown.

Experimental validation of PSK in PWC. As second proof-of-concept experiment, we consider PWC with phase shift keying (PSK) (de)modulation. Unlike PSK in AWC, binary PSK here means that the calibrated coherence coefficient $\widehat{H}_{s\to meta\to mr}$ has two opposite phase states, i.e., 0 and π. Similar to above (**Figure 2a**), we consider three-channel PWC. We obtain offline 8 coding patterns for controlling the metasurface by solving the constrained optimization problem in equation (4) using the algorithm provided in **Supplementary Note 4**. Then, we build a three-channel PWC-BPSK modulation scheme, and report the obtained results in **Figure 3a**. Amplitude and phase distributions of $\widehat{H}_{s\to meta\to mr}$ at the distance of z=3m away from the metasurface are reported in **Figure 3b-c**. Note that the intensities of $|\widehat{H}_{s\to meta\to mr}|$ are focused around the three users, and the phases of $\widehat{H}_{s\to meta\to mr}$ are well controlled in the desired manner. Clearly, we can see that the three-channel PWC-BPSK modulation is easily achieved by electronically switching the coding patterns of the metasurface, and that the sequence of BPSK digital information can be independently controlled for each channel. Based on these 8 PWC-BPSK coding patterns, we realize PWC transmission of a full-color image from Alice to Bob at the distance of 3m away from the metasurface. The corresponding experimental results are provided in **Figure 4**, where the wireless signals are acquired with the four-port oscilloscope. Again, we can see that the three monochrome images can be transferred independently to three users with high communication quality.

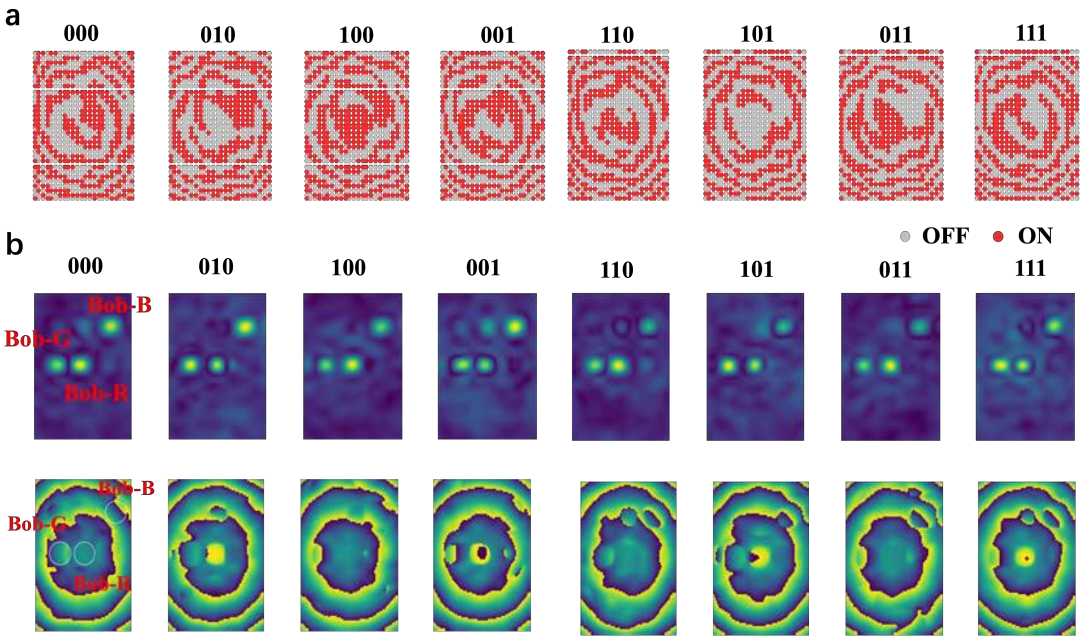

c

Amplitudes and Phases of 3-channel BPSK for the optimized 8 coding patterns

	Bob-R		Bob-G		Bob-B	
Code	**Amplitude**	**Phase**	**Amplitude**	**Phase**	**Amplitude**	**Phase**
"000"	1.50	5.71	1.55	-16.52	1.52	3.63
"100"	1.46	178.12	1.45	-9.37	1.45	4.10
"010"	1.56	6.38	1.56	-173.93	1.56	0.56
"110"	1.33	-172.98	1.32	179.56	1.32	2.58
"001"	1.38	11.67	1.38	-20.32	1.38	176.47
"101"	1.33	176.46	1.31	-12.38	1.32	173.29
"011"	1.43	5.01	1.43	-168.71	1.44	175.95
"111"	1.22	179.04	1.20	-178.68	1.23	176.95

d

Parameter	Value
Wi-Fi working frequency	2.442Ghz
Wi-Fi protocol	802.11a/b/g
Wi-Fi router model	TL-WDR5620
Modulation method	BPSK
Sampling rate	40Mbps
Transmission rate	500Kbps
Frame size	816000 samples
PerFrame size	320*320pixe
Bit error Rat	0.005
Transmit power	-10dbm
Receiver Gain	20dbm

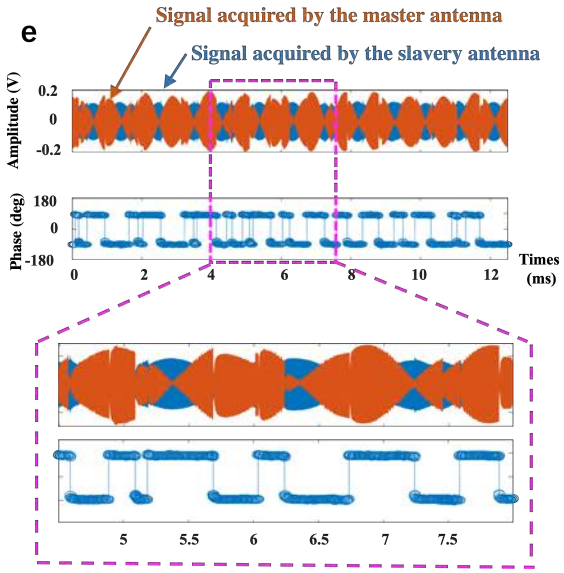

Figure 3. Results of the three-channel binary PSK PWC. a, Optimized coding patterns for the three-channel PWC-BASK. **b,** Amplitude (top) and phase (bottom) distributions of $H_{s\to meta\to mr}$, corresponding to the 8 coding patterns plotted in **a,** at 2.424 GHz. Amplitude and phase of information-carrying stray Wi-Fi signals can be well controlled for the purpose of passive phase modulation. **c,** Experimentally measured amplitudes and phases on Bob's side for the optimized 8 different coding patterns. **d,** Selected key parameters of the designed USRP-based PWC demo system. **e**, (top) the stray Wi-Fi signals with about 12ms length, which are acquired by the master (red line) and slavery (blue line) antennas, (bottom) the corresponding phase by the proposed PWC demodulation method. Further, the signal parts within the range of 4-8ms marked in purple are enlarged at the bottom.

In order to give a more realistic demonstration, we consider the transmission of a color-scale video to Bob-R, and provide experimental results in **Supplementary Video 1**. In this experiment, a software-defined radio (Ettus USRP X310) with two commercial electronically-small antennas is utilized to acquire the stray Wi-Fi signals modulated by PWC-BPSK. Now, we can clearly see that the information sequence encoded into the metasurface can be smoothly and "sneakily" transferred from Alice to Bob with a data rate of 500Kbps – without affecting the background active Wi-Fi communication. Selected information on the fabricated demo system is provided in **Figures 3d** and **3e**. More details about the demo can found in **Supplementary Note 8**.

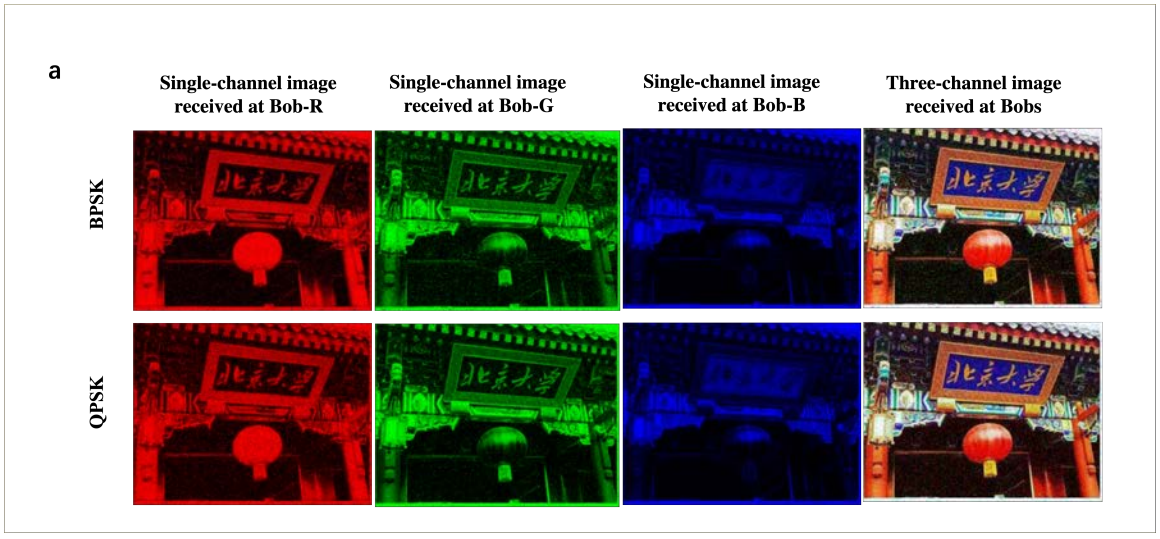

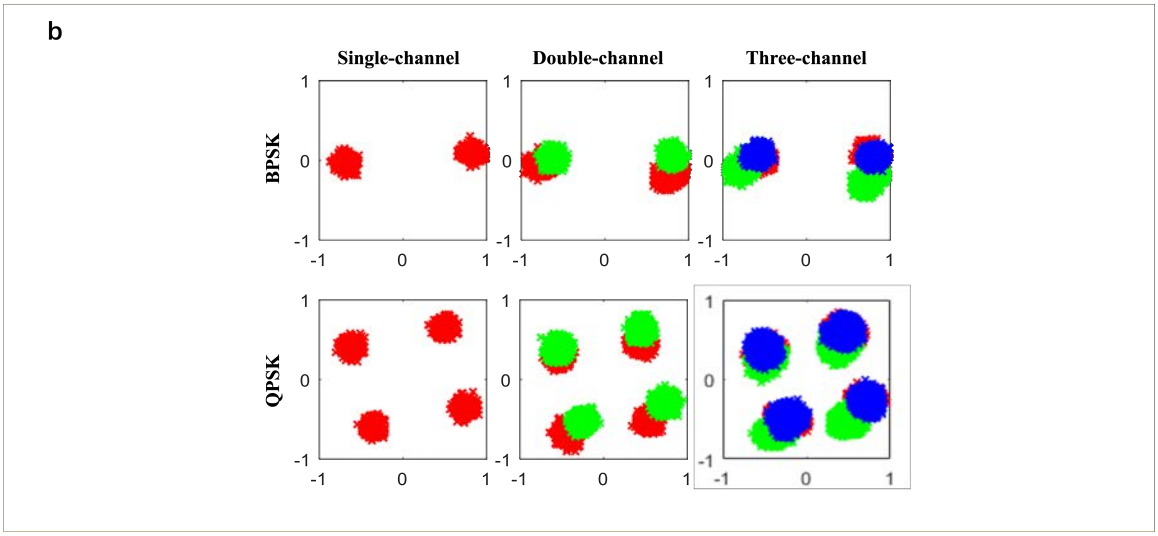

Figure 4. Results of the BPSK PWC and QPSK PWC. a, Individual monochrome and synthesized full-color images transmitted from Alice to Bob by PWC-BPSK and PWC-QPSK. **b,** Constellation results of PWC-BPSK and PWC-QPSK.

As third and final proof-of-concept experiment, we demonstrate PWC with quadrature PSK (QPSK) (de)modulation. The constellation results of PWC-BPSK and PWC-QPSK are compared in **Figure 4a**. All four states are clearly distinguishable, the corresponding clouds in the complex plane do not overlap. Ref.[35] suggests that similar results can also be achieved in more strongly reverberating indoor environments. The experimental results for a full-color image transfer with PWC BPSK and PWC-QPSK are shown in **Figure 4b**.

Conclusion

In summary, we introduced the concept of PWC, we provided a theoretical framework for encoding/decoding and modulation/demodulation, and we built several proof-of-principle prototype systems tailored to the use of ambient commodity 2.4GHz Wi-Fi signals. In contrast to conventional AWC which relies on an actively generated carrier, the proposed PWC is based on the modulation of already existing stray ambient electromagnetic signals with a programmable metasurface whose configurations encode digital information directly on the physical level. Our results demonstrate PWC with data rates on the order of

hundreds of Kbps without requiring an active radiofrequency chain, energy and spectral resources to generate a carrier signal. Therefore, the reported PWC strategy has the potential to fundamentally resolve pressing issues in conventional AWC (energy consumption, spectrum allotment, hardware cost, information security), notably in the context of green IoT connectivity. We believe that our PWC strategy provides a fundamentally new view on wireless communication that can impact a wide range of future communication systems at radiofrequencies and beyond.

Materials and Methods

Programmable metasurface. The designed 1-bit electronically-controllable meta-atom is detailed in **Supplementary Note 5**. The meta-atom is composed of two substrate layers, and the top square patch is integrated with a SMP1345-079LF PIN diode. The top square patch size is $54\times 54\text{mm}^2$, the thickness of the top substrate F4BM with the relative permittivity of 2.55 and the loss tangent of 0.0015 and the bottom substrate FR-4 has the thickness of 0.7mm. **Supplementary Figures 2b-c** report the experimental phase and amplitude response of a unit cell as function of frequency for different unit cell configurations. The phase response changes by 180° around 2.4GHz when the PIN is switched from OFF (ON) to ON (OFF), while the amplitudes remains almost unaltered (above 85%). The designed metasurface can to reshape the spatial distribution of ambient stray Wi-Fi waves.

Information encoding/decoding and modulation/demodulation. As detailed in **Supplementary Note 1**, the demodulated signal $H_{s\to meta\to mr}$ which conveys the digital information can be approximately expressed as

$$H_{s\to meta\to mr}(\boldsymbol{r}_m,\omega,\mathcal{C}) \approx \sum_{n=1}^{N}\sigma(\boldsymbol{r}_n,\mathcal{C})G(\boldsymbol{r}_n,\boldsymbol{r_m},\omega), \quad (5)$$

where $\sigma(\boldsymbol{r}_n,\mathcal{C})$ denotes the reflection coefficient of the meta-atom at $\boldsymbol{r}_n$ when the metasurface is controlled with the coding pattern $\mathcal{C}$, $G(\boldsymbol{r}_n,\boldsymbol{r_m},\omega)$ is the Green's function

imposed by the surrounding medium, $\boldsymbol{r}_m$ is the location of the master receiver, and N is the total number of meta-atoms. $H_{s\to meta\to mr}(\boldsymbol{r}_m, \omega, \mathcal{C})$ approximately equals the signal radiated from the programmable metasurface with coding pattern $\mathcal{C}$. $H_{s\to meta\to mr}$ can be designed to have a finite number of well-distinguishable digital states by optimizing the coding patterns of the metasurface. These distinguishable digital states can be recognized by using a classifier or decoder. Moreover, equation (5) implies that $H_{s\to meta\to mr}$ can be designed to be radiation-direction-dependent, such that the information retrieved by different users can be independently controlled. In the far-field approximation, the smallest achievable size of the focal spot around the master receiver is on the order of $O(\lambda R/D)$, where λ denotes the operational wavelength, R is the communication distance, and D is the size of the metasurface aperture. Focusing on the master receiver(s) is crucial to ensures a high SNR of the demodulated signal by harvesting the energy of stray Wi-Fi waves for PWC. We have performed an additional analysis of channel strength and transmission efficiency which is detailed in **Supplementary Note 6**.

Author Contribution

L.L. conceived the idea, conducted the theoretical analysis and wrote the paper. H. Z. built the proof-of-principle prototype system, Y. S. and H. Z. conducted experiments and data processing. P.d.H. contributed to conceptualization and write-up of the project. All authors participated in the data analysis and read the manuscript.

Additional Information

Supplementary Information accompanies this article.

Competing Interests: The authors declare no competing financial interests.

References

1. Sarkar, T. K. & Baker, D. C. *History of Wireless*. (Wiley-Interscience, 2006).

2. Proakis, J. G. *Digital Communications.* (McGraw-Hill, 2001).
3. Goldsmith, A. *Wireless Communications*. (Cambridge University Press, 2005).
4. Shannon, C. E. A mathematical theory of communication. *Bell Syst. Tech. J.* **27**, 379–423 (1948).
5. Foschini, G. J. & Gans, M. J. On limits of wireless communications in a fading environment when using multiple antennas. *Wirel. Pers. Commun.* **6**, 311–335 (1998).
6. Cho, Y. S., Kim, J., Yang, W. Y. & Kang, C. *MIMO-OFDM wireless communications with MATLAB*. (Wiley-IEEE Press, 2011).
7. Marzetta, T. L. Massive MIMO: An Introduction. *Bell Labs Tech. J.* **20**, 11–22 (2015).
8. del Hougne, P., Fink, M. & Lerosey, G. Optimally diverse communication channels in disordered environments with tuned randomness. *Nat. Electron.* **2**, 36–41 (2019).
9. Cui, T. J., Qi, M. Q., Wan, X., Zhao, J. & Cheng, Q. Coding metamaterials, digital metamaterials and programmable metamaterials. *Light Sci. Appl.* **3**, e218–e218 (2014).
10. Li, L. & Cui, T. J. Information metamaterials – from effective media to real-time information processing systems. *Nanophotonics* **8**, 703–724 (2019).
11. Ou, J.-Y., Plum, E., Zhang, J. & Zheludev, N. I. An electromechanically reconfigurable plasmonic metamaterial operating in the near-infrared. *Nature Nanotech* **8**, 252–255 (2013).
12. Rout, S. & Sonkusale, S. Wireless multi-level terahertz amplitude modulator using active metamaterial-based spatial light modulation. *Opt. Express* **24**, 14618 (2016).
13. Arbabi, E. *et al.* MEMS-tunable dielectric metasurface lens. *Nat Commun* **9**, 812 (2018).
14. Huang, D., Nandakumar, R. & Gollakota, S. Feasibility and Limits of Wi-Fi Imaging. *Proceedings of the 12th ACM conference on embedded network sensor systems* 266–279 (2014).
15. Garnier, J. & Papanicolaou, G. *Passive Imaging with Ambient Noise*. (Cambridge University Press, 2016).

16. Holl, P. M. & Reinhard, F. Holography of Wi-fi Radiation. *Phys. Rev. Lett.* **118**, 183901 (2017).

17. Palmer, J. *et al.* Receiver platform motion compensation in passive radar. *IET Radar, Sonar & Navigation* **11**, 922–931 (2017).

18. Feng, W., Friedt, J.-M., Hu, Z., Cherniak, G. & Sato, M. WiFi-based imaging for ground penetrating radar applications: fundamental study and experimental results. *The Journal of Engineering* **2019**, 6364–6368 (2019).

19. Watts, C. M. *et al.* Terahertz compressive imaging with metamaterial spatial light modulators. *Nat. Photon.* **8**, 605–609 (2014).

20. Sleasman, T., F. Imani, M., Gollub, J. N. & Smith, D. R. Dynamic metamaterial aperture for microwave imaging. *Appl. Phys. Lett.* **107**, 204104 (2015).

21. del Hougne, P., Imani, M. F., Fink, M., Smith, D. R. & Lerosey, G. Precise Localization of Multiple Noncooperative Objects in a Disordered Cavity by Wave Front Shaping. *Phys. Rev. Lett.* **121**, 063901 (2018).

22. Li, L. *et al.* Machine-learning reprogrammable metasurface imager. *Nat. Commun.* **10**, 1082 (2019).

23. del Hougne, P., Imani, M. F., Diebold, A. V., Horstmeyer, R. & Smith, D. R. Learned Integrated Sensing Pipeline: Reconfigurable Metasurface Transceivers as Trainable Physical Layer in an Artificial Neural Network. *Adv. Sci.* 1901913 (2019) doi:10.1002/advs.201901913.

24. Li, L. *et al.* Intelligent metasurface imager and recognizer. *Light Sci. Appl.* **8**, 97 (2019).

25. Li, H.-Y. *et al.* Intelligent Electromagnetic Sensing with Learnable Data Acquisition and Processing. *Cell Patterns (in press).*

26. Yoo, I., Imani, M. F., Sleasman, T., Pfister, H. D. & Smith, D. R. Enhancing Capacity of Spatial Multiplexing Systems Using Reconfigurable Cavity-Backed Metasurface Antennas in Clustered MIMO Channels. *IEEE Trans. Commun.* **67**, 1070–1084 (2019).

27. Renzo, M. D. *et al.* Smart radio environments empowered by reconfigurable AI meta-

surfaces: an idea whose time has come. *J Wireless Com Network* **2019**, 129 (2019).

28. Hu, S., Rusek, F. & Edfors, O. Beyond Massive MIMO: The Potential of Data Transmission With Large Intelligent Surfaces. *IEEE Trans. Signal Process.* **66**, 2746–2758 (2018).
29. Zhao, J. *et al.* Programmable time-domain digital-coding metasurface for non-linear harmonic manipulation and new wireless communication systems. *National Science Review* **6**, 231–238 (2019).
30. Zhang, L. *et al.* Space-time-coding digital metasurfaces. *Nat. Commun.* **9**, 4334 (2018).
31. Cui, T. J., Liu, S., Bai, G. D. & Ma, Q. Direct Transmission of Digital Message via Programmable Coding Metasurface. *Research* **2019**, 1–12 (2019).
32. Li, L. *et al.* Electromagnetic reprogrammable coding-metasurface holograms. *Nat. Commun.* **8**, 197 (2017).
33. del Hougne, P., Fink, M. & Lerosey, G. Shaping Microwave Fields Using Nonlinear Unsolicited Feedback: Application to Enhance Energy Harvesting. *Phys. Rev. Applied* **8**, 061001 (2017).
34. Smith, D. R. *et al.* An analysis of beamed wireless power transfer in the Fresnel zone using a dynamic metasurface aperture. *Journal of Applied Physics* **121**, 014901 (2017).
35. del Hougne, P. & Lerosey, G. Leveraging Chaos for Wave-Based Analog Computation: Demonstration with Indoor Wireless Communication Signals. *Phys. Rev. X* **8**, 041037 (2018).
36. Neyman, J. & Pearson, E. S. On the problem of the most efficient tests of statistical hypotheses. *Phil. Trans. Roy. Soc. A* **231**, 694–704 (1933).
37. Neyman, J. & Pearson, E. S. The testing of statistical hypotheses in relation to probabilities a priori. *Math. Proc. Camb. Phil. Soc.* **29**, 492–510 (1933).